An efficient method for hybrid density functional calculation with spin-orbit coupling

Maoyuan Wang,[1, 2] Gui-Bin Liu,[1, *] Hong Guo,[2] and Yugui Yao[1, †]

[1]*Beijing Key Laboratory of Nanophotonics and Ultrafine Optoelectronic Systems,*
School of Physics, Beijing Institute of Technology, Beijing 100081, China
[2]*Department of physics, McGill University, Montreal, H3A 2T8, Canada*
(Dated: September 11, 2018)

In first-principles calculations, hybrid functional is often used to improve accuracy from local exchange correlation functionals. A drawback is that evaluating the hybrid functional needs significantly more computing effort. When spin-orbit coupling (SOC) is taken into account, the non-collinear spin structure increases computing effort by at least eight times. As a result, hybrid functional calculations with SOC are intractable in most cases. In this paper, we present an approximate solution to this problem by developing an efficient method based on a mixed linear combination of atomic orbital (LCAO) scheme. We demonstrate the power of this method using several examples and we show that the results compare very well with those of direct hybrid functional calculations with SOC, yet the method only requires a computing effort similar to that without SOC. The presented technique provides a good balance between computing efficiency and accuracy, and it can be extended to magnetic materials.

I. INTRODUCTION

Density functional theory (DFT) is a powerful method for predicting properties of materials such as crystal structures, electronic bands, phonon dispersions and other physical quantities. Practically, using appropriate exchange correlation (XC) functional is very important for accuracy, especially for predicting band gaps of materials. It is well known that the local density approximation (LDA) and general gradient approximation (GGA) XC functionals tend to severely underestimate band gaps [1]. Consequently, hybrid functionals (HF) such as PBE0 [2–5], HSE03 and HSE06 [6–9] were proposed and they often predict very good band gap values comparable to experiments. A drawback of HF is that it needs very significant computing resources, generally several orders of magnitude more compared to that of LDA or GGA.

In recent years, materials with strong spin-orbit coupling (SOC) have attracted great attention, including topological insulators [10, 11] Bi_2Se_3 [12], silicene [13, 14], germanene [13, 14], stanene [13–15], BiH [16, 17], $ZrTe_5$ [18], Bi_4Br_4 [19], ZrSiO [20], photoelectric materials PbI_2 [21] and BiOCl [22], two-dimensional group-VI_B transition metal dichalcogenides MoS_2, $MoSe_2$, WS_2, and WSe_2 [23], III_A-V_A direct band-gap semiconductors with heavy elements GaSb and InSb [24], etc. DFT calculations including SOC involve non-collinear spin which requires at least eight times more computing time as compared to that without SOC, due to the $O(N^3)$ scaling for solving the Kohn-Sham DFT equations (KS-DFT). Since many of these SOC materials are semiconductors, HF calculations are desired to more accurately predict their band gaps and electronic structures. Unfortunately, HF+SOC calculations are numerically intractable thus

rarely used - unless the unit cell is extremely small, due to the huge computational demand. It is the purpose of this paper to report a practical solution to this problem.

In particular, we propose an efficient approximate technique for HF+SOC calculations based on a mixed linear combination of atomic orbital (LCAO) scheme. The mixed LCAO Hamiltonian is constructed by two parts: an SOC-free part whose parameters are obtained from HF calculations without SOC, and an SOC part whose parameters are obtained from GGA+SOC calculations (DFT at the GGA level with SOC). Applying this approach to several non-magnetic materials, the results are demonstrated to be very close to those of direct HF+SOC calculation and much more accurate than the GGA+SOC calculation. Importantly, the required computing time of the mixed LCAO technique is comparable to that of HF calculation without SOC.

In the rest of the work, the DFT calculations are performed using the projector augmented wave method implemented in VASP [25]. The Perdew-Burke-Ernzerhof (PBE) parametrization of GGA functional [26, 27] and Heyd-Scuseria-Ernzerh hybrid functional (HSE06) [6–9] are used in the DFT calculations, and the VASP2WANNIER90 interface [28–30] is used to obtain the LCAO parameters from the DFT results. Since numerical calculations are for the purpose of demonstrating the mixed LCAO technique, structure optimization is omitted.

II. THE METHOD

WANNIER90 [28, 29] is used to construct LCAO or Wannier-bases Hamiltonian from DFT calculations, and the resulting LCAO Hamiltonian can reproduce the original energy dispersion very well. We start by construct-

ing an LCAO Hamiltonian to treat HF+SOC using DFT calculations.

For a given system, the required computing effort is most demanding for HF+SOC, followed by HF without SOC and next followed by GGA+SOC. Clearly and as explained in the Introduction, if HF+SOC were computationally affordable in general, the work of this paper would not be necessary. That is not the case. In the following we utilize HF without SOC and GGA+SOC to construct a mixed LCAO Hamiltonian H^{MIX} which we show to be a very good approximation to $H^{\mathrm{HF+SOC}}$. In particular, H^{MIX} has two terms, H_0^{HF} which is obtained from HF without SOC, and $H_{\mathrm{so}}^{\mathrm{GGA}}$ which is obtained from GGA+SOC,

$$H^{\mathrm{MIX}} = H_0^{\mathrm{HF}} + H_{\mathrm{so}}^{\mathrm{GGA}}. \quad (1)$$

Clearly, constructing H^{MIX} only consumes a time that is comparable to HF without SOC, thus much more efficient than that of a full HF+SOC calculation. The fact that H^{MIX} compare very well with direct HF+SOC calculations (see below), suggests that the mixed LCAO scheme provides a viable approximation for the complicated HF+SOC analysis.

On the technical side, while H_0^{HF} can be constructed directly from DFT calculation of HF without SOC, $H_{\mathrm{so}}^{\mathrm{GGA}}$ is obtained from DFT of GGA+SOC involving a procedure for separating out the SOC contributions. The latter procedure and an associated technical detail are discussed in the following two subsections.

A. Separating out the SOC contribution

The Hamiltonian H of SOC systems can be divided into a non-SOC term H_0 plus the SOC term H_{so}:

$$H = H_0 + H_{\mathrm{so}}. \quad (2)$$

In LCAO representation, H_0 involves on-site energy and hopping integral between different atomic orbitals, and H_{so} comes from SOC effects.

In the spin-up and spin-down bases $|\uparrow\rangle$ and $|\downarrow\rangle$, the non-SOC term H_0 can be written as a diagonal 2×2 matrix:

$$H_0 = \begin{pmatrix} H_0^\uparrow & 0 \\ 0 & H_0^\downarrow \end{pmatrix}. \quad (3)$$

For simplicity, we consider non-magnetic systems in the rest of this work, but extension to magnetic system can be readily made without fundamental difficulty. For non-magnetic materials, $H_0^\uparrow = H_0^\downarrow$.

For the SOC term H_{so}, its original operator form is:

$$H_{\mathrm{so}} = \frac{\hbar}{4m_0^2 c^2} \left(\nabla V \times \boldsymbol{p} \right) \cdot \boldsymbol{s} \equiv \xi \boldsymbol{\mathcal{L}} \cdot \boldsymbol{s}, \quad (4)$$

where $\hbar$ is the reduced Planck constant, m_0 is the bare mass of electron, c is the velocity of light, $V(\boldsymbol{r})$ is the potential energy, $\boldsymbol{p}$ the momentum, and $\boldsymbol{s}$ the vector of Pauli matrices representing the spin degrees of freedom. For clarity we define a constant $\xi \equiv \hbar/(4m_0^2 c^2)$ and a vector operator $\boldsymbol{\mathcal{L}} \equiv \nabla V \times \boldsymbol{p}$. H_{so} can then be rewritten in the following matrix form:

$$\begin{aligned} H_{\mathrm{so}} &= \xi(\mathcal{L}_x s_x + \mathcal{L}_y s_y + \mathcal{L}_z s_z) \\ &= \xi \begin{pmatrix} \mathcal{L}_z & \mathcal{L}_x - i\mathcal{L}_y \\ \mathcal{L}_x + i\mathcal{L}_y & -\mathcal{L}_z \end{pmatrix} \equiv \begin{pmatrix} H_{\mathrm{so}}^{\uparrow\uparrow} & H_{\mathrm{so}}^{\uparrow\downarrow} \\ H_{\mathrm{so}}^{\downarrow\uparrow} & H_{\mathrm{so}}^{\downarrow\downarrow} \end{pmatrix}, \quad (5) \end{aligned}$$

in which $H_{\mathrm{so}}^{\downarrow\downarrow} = -H_{\mathrm{so}}^{\uparrow\uparrow}$ and $H_{\mathrm{so}}^{\downarrow\uparrow} = H_{\mathrm{so}}^{\uparrow\downarrow\dagger}$.

According to Eq. 2 to Eq. 5, the total Hamiltonian for a non-magnetic system with SOC is:

$$H \equiv \begin{pmatrix} H_{11} & H_{12} \\ H_{21} & H_{22} \end{pmatrix} = \begin{pmatrix} H_0^\uparrow & 0 \\ 0 & H_0^\uparrow \end{pmatrix} + \begin{pmatrix} H_{\mathrm{so}}^{\uparrow\uparrow} & H_{\mathrm{so}}^{\uparrow\downarrow} \\ H_{\mathrm{so}}^{\uparrow\downarrow\dagger} & -H_{\mathrm{so}}^{\uparrow\uparrow} \end{pmatrix}. \quad (6)$$

Then, from Eq. 6, we can separate the total Hamiltonian H to obtain H_0 and H_{so} as the following:

$$H_0 = \begin{pmatrix} \left(H_{11} + H_{22}\right)/2 & 0 \\ 0 & \left(H_{11} + H_{22}\right)/2 \end{pmatrix}, \quad (7)$$

$$H_{\mathrm{so}} = \begin{pmatrix} \left(H_{11} - H_{22}\right)/2 & H_{12} \\ H_{21} & -\left(H_{11} - H_{22}\right)/2 \end{pmatrix}. \quad (8)$$

Hence, after obtaining the LCAO Hamiltonian $H^{\mathrm{GGA+SOC}}$ from the corresponding DFT calculation, its SOC part $H_{\mathrm{so}}^{\mathrm{GGA}}$ can be separated out using Eq.8.

B. Mixing the Hamiltonian

With the obtained non-SOC part H_0^{HF} and SOC part $H_{\mathrm{so}}^{\mathrm{GGA}}$, the mixed LCAO Hamiltonian H^{MIX} that approximates HF+SOC is determined by Eq.1. Hereinafter we use the HSE functional for HF, and PBE functional for GGA. Then Eq.1 becomes

$$H^{\mathrm{MIX}} = H_0^{\mathrm{HSE}} + H_{\mathrm{so}}^{\mathrm{PBE}}. \quad (9)$$

The "mixing" procedure appears to be a simple addition. However it should be noted that only when H_0^{HSE} and $H_{\mathrm{so}}^{\mathrm{PBE}}$ are constructed under the same bases can they be added directly. We achieve this by constructing H_0^{HSE} and $H_{\mathrm{so}}^{\mathrm{PBE}}$ in the same bases $|\tilde{\varphi}_{m\boldsymbol{k}}\rangle$, and details are presented in the appendix A. This way, we finally constructed the mixed Hamiltonian H^{MIX} to treat HSE+SOC.

III. RESULTS, ANALYSIS AND DISCUSSION

Having constructed H^{MIX} to efficiently treat HSE+SOC, in this section we demonstrate its accuracy using several material systems. Predicting band
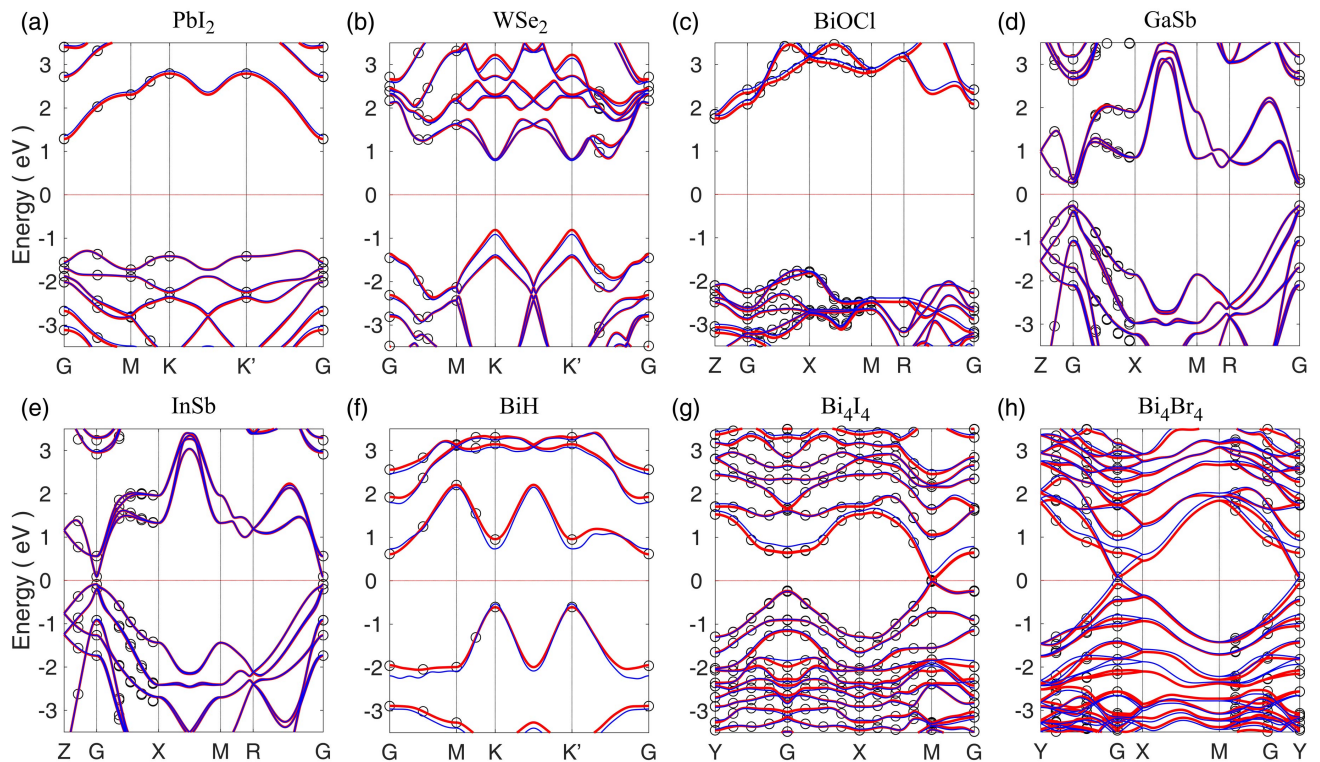
FIG. 1. **Comparison of band structures for the example materials.** In each band structure, black circles are the results from direct HSE+SOC DFT calculation; red thick lines are the reproduced HSE+SOC bands by LCAO fitting; and blue thin lines are results of our method, i.e. H^{MIX} in Eq. 9.

gap is important, which is one of the reasons to use HSE in the first place[6–9]. We calculated band gaps for eight semiconductor materials having heavy elements thus large SOC, including two-dimensional (2D) mono-layers of PbI_2, WSe_2, BiH, Bi_4I_4 and Bi_4Br_4; 3D crystals BiOCl, GaSb, and InSb [24]. The SOC effect is important for these materials, especially for their band gaps.

For the eight materials, we performed (very time-consuming) direct HSE+SOC calculations and using the results, we constructed an LCAO Hamiltonian $H^{\mathrm{HSE+SOC}}$: this would not be possible without the full direct HSE+SOC calculation. Then, we constructed H^{MIX} following the procedure in the last section which does not require full HSE+SOC calculation. The three sets of results are compared: direct numerical data from full HSE+SOC calculations and from $H^{\mathrm{HSE+SOC}}$, as well as from H^{MIX}.

First, band structures of the eight compounds calculated by our method via H^{MIX} of Eq.9 is plotted in Fig.1, together with those from the direct HSE+SOC calculation and its fitting $H^{\mathrm{HSE+SOC}}$. The full HSE+SOC data are presented in black circles and the bands from $H^{\mathrm{HSE+SOC}}$ are in thick red lines: these are used as benchmarks to compare to our results by H^{MIX} which are presented in thin blue lines. We can see that the bands cal-

culated by our method via H^{MIX} of Eq.9 (thin blue lines) are qualitatively consistent to the benchmark results for all cases. In particular, band dispersions by H^{MIX} and the benchmark $H^{\mathrm{HSE+SOC}}$ agree well for PbI_2, WSe_2, GaSb, and InSb; and the agreement is somewhat reduced for BiOCl, BiH, Bi_4I_4, and Bi_4Br_4. In the latter cases, although the heavy element Bi gives rise to some quantitative difference, there is no qualitative discrepancy for the full range of the Brillouin zone.

Second, quantitatively we compare the band gaps of H^{MIX} and the benchmark $H^{\mathrm{HSE+SOC}}$ in Table I. The band gaps obtained by H^{MIX} are close to those of the benchmark $H^{\mathrm{HSE+SOC}}$ for five of the eight compounds PbI_2, WSe_2, BiOCl, GaSb, and InSb [see the column labeled by $|\Delta_1|/g(H^{\mathrm{HSE}}_{+\mathrm{SOC}})$ column in Table I]. But for three compounds BiH, Bi_4I_4 and Bi_4Br_4 - especially Bi_4I_4 which has a very small band gap, the discrepancy is large. As a supplement, we also show the calculated band gaps by PBE+SOC in Table I: they are not only quantitatively quite different from the benchmark results, two of them are even qualitatively wrong (GaSb, InSb).

As for the three compounds with band gaps of H^{MIX} showing large discrepancy to the benchmark, BiH, Bi_4I_4 and Bi_4Br_4, they are all relevant to topological insulators which exhibit band inversion near the Fermi level when SOC is considered and have normal bands with

TABLE I. **Comparison of band gaps** (in unit of eV) from different Hamiltonians $H^{\text{HSE}}_{+\text{SOC}}$, H^{MIX}, $H^{\text{PBE}}_{+\text{SOC}}$, and $\tilde{H}^{\text{MIX}}$, in which $H^{\text{HSE(PBE)}}_{+\text{SOC}}$ is an alternative denotion of $H^{\text{HSE(PBE)+SOC}}$ due to the space limit in table and $\tilde{H}^{\text{MIX}}$ is defined as $\tilde{H}^{\text{MIX}} = \tilde{H}^{\text{HSE}}_0 + H^{\text{PBE}}_{\text{so}}$ (for $\tilde{H}^{\text{HSE}}_0$ see eq. 10 for details). The band gap of a Hamiltonian h is denoted as $g(h)$. $\Delta_1 = g(H^{\text{MIX}}) - g(H^{\text{HSE}}_{+\text{SOC}})$, $\Delta_2 = g(\tilde{H}^{\text{MIX}}) - g(H^{\text{HSE}}_{+\text{SOC}})$, and absolute relative deviations are also shown in percentages. For BiH, the gap we list here is the band gap opened by SOC at the Dirac point $K(K')$ [16, 17]. For GaSb and InSb, PBE+SOC calculations give wrong metallic results with no gaps.

	$g(H^{\text{HSE}}_{+\text{SOC}})$	$g(H^{\text{MIX}})$	$g(H^{\text{PBE}}_{+\text{SOC}})$	Δ_1	$|\Delta_1|/g(H^{\text{HSE}}_{+\text{SOC}})$	$g(\tilde{H}^{\text{MIX}})$	Δ_2	$|\Delta_2|/g(H^{\text{HSE}}_{+\text{SOC}})$
PbI_2	2.569	2.648	1.862	0.079	3.08%	2.626	0.057	2.22%
WSe_2	1.619	1.702	1.247	0.083	5.13%	1.703	0.084	5.19%
BiOCl	3.496	3.556	2.511	0.060	1.72%	3.502	0.006	0.17%
GaSb	0.526	0.527	Metal	0.001	0.19%	0.531	0.005	0.95%
InSb	0.175	0.174	Metal	−0.001	0.57%	0.182	0.007	4.00%
BiH	1.567	1.267	1.252	−0.300	19.10%	1.260	−0.307	19.60%
Bi_4I_4	0.020	0.206	0.170	0.186	930.0%	0.202	0.182	910.0%
Bi_4Br_4	0.166	0.021	0.357	−0.145	87.35%	0.047	−0.119	71.69%

SOC not considered. Concretely, 2D monolayers of BiH and Bi_4Br_4 are topological insulators[19]. As for Bi_4I_4 monolayer, although it is not a topological insulator, it lies near the transition point between normal and topological insulator which makes it also sensitive to SOC. The impact of topological properties on the accuracy of our method needs to be analyzed.

Recall that we used $H^{\text{MIX}} = H^{\text{HSE}}_0 + H^{\text{PBE}}_{\text{so}}$ to approximate $H^{\text{HSE+SOC}}$ which can be written as

$$H^{\text{HSE+SOC}} = \tilde{H}^{\text{HSE}}_0 + H^{\text{HSE}}_{\text{so}} \qquad (10)$$

where $\tilde{H}^{\text{HSE}}_0$ and $H^{\text{HSE}}_{\text{so}}$ were obtained directly from $H^{\text{HSE+SOC}}$ using Eq.7 and Eq.8, respectively. Therefore, any discrepancy between H^{MIX} and $H^{\text{HSE+SOC}}$ has two sources: (i) the discrepancy between the non-SOC part H^{HSE}_0 (obtained from HSE without SOC) and $\tilde{H}^{\text{HSE}}_0$; (ii) the discrepancy between the SOC part $H^{\text{PBE}}_{\text{so}}$ and $H^{\text{HSE}}_{\text{so}}$. We analyze these terms in the next two subsections.

A. HSE without SOC

In this subsection we analyze the source of discrepancy in the non-SOC part H^{HSE}_0 (obtained from HSE without SOC) and $\tilde{H}^{\text{HSE}}_0$. Since DFT is based on ground state electronic density, any discrepancy should be due to the difference between densities calculated by the two approaches [31]. To illustrate this, we proceed by making use of a model Hamiltonian as follows:

$$\begin{aligned}
H = &\sum_c \varepsilon_{0c} a^\dagger_c a_c + \sum_v \varepsilon_{0v} a^\dagger_v a_v \\
&+ \sum_{c,c'} \xi^{\text{SO}}_{c,c'} a^\dagger_c a_{c'} + \sum_{v,v'} \xi^{\text{SO}}_{v,v'} a^\dagger_v a_{v'} \\
&+ \sum_{c,v} (\xi^{\text{SO}}_{c,v} a^\dagger_c a_v + \text{h.c.})
\end{aligned} \qquad (11)$$

where the first and second terms are the non-SOC part H_0, the third to fifth terms — denoted as $H^{\text{SO}}_{\text{c,c}}$, $H^{\text{SO}}_{\text{v,v}}$, and $H^{\text{SO}}_{\text{c,v}}$ respectively, constitute the SOC part H_{so}. In Eq.11, $a_{c(v)}$ and $a^\dagger_{c(v)}$ are respectively annihilation and creation operators for the c conduction (v valence) band[32] eigenstate ψ_{0c} (ψ_{0v}) of H_0 whose eigenenergy is ε_{0c} (ε_{0v}).

The Hamiltonian in Eq.11 can be analyzed by perturbation theory. We take the non-SOC H_0 as the unperturbed Hamiltonian and the SOC term H_{so} as the perturbation. Note that $H_{\text{so}} = H^{\text{SO}}_{\text{c,c}} + H^{\text{SO}}_{\text{v,v}} + H^{\text{SO}}_{\text{c,v}}$ can be divided into two types according to their SOC effects: $H^{\text{SO}}_{\text{c,c}}$ and $H^{\text{SO}}_{\text{v,v}}$ are the "type-I" terms, $H^{\text{SO}}_{\text{c,v}}$ is the "type-II" term. The type-I term $H^{\text{SO}}_{\text{c,c}} + H^{\text{SO}}_{\text{v,v}}$ couples conduction bands with other conduction bands as well as valence bands with other valence bands. We distinguish two situations. (i) If the unperturbed band gap is large relative to the type-I SOC effect, the type-I term only splits bands and no band crossing occurs. This is the "weak type-I SOC" which does not make any significant difference between the unperturbed and perturbed charge densities (see Appendix B for details). (ii) If the unperturbed band gap is small relative to the type-I SOC effect, some split bands near the band gap will cross the Fermi level so that the charge density is altered. This is the "strong type-I SOC" [cf. Fig. 2(b)].

As for the type-II SOC $H^{\text{SO}}_{\text{c,v}}$, it mixes valence bands with conduction bands, for instance the first-order perturbed valence band state ψ_v is

$$\psi_v \approx \frac{1}{C}(\psi_{0v} + \sum_c \alpha_c \psi_{0c}), \qquad (12)$$

in which $\alpha_c = \xi^{\text{SO}}_{c,v}/(\varepsilon_{0v} - \varepsilon_{0c})$ and C is a normalization constant. As a result, the type-II SOC term alters charge density via the sum of all occupied states, i.e. all valence band states in the presence of band gap [cf. Fig. 2(c)].

Let us first understand why for the five normal band insulators PbI_2, BiOCl, WSe_2, GaSb and InSb, H^{MIX}
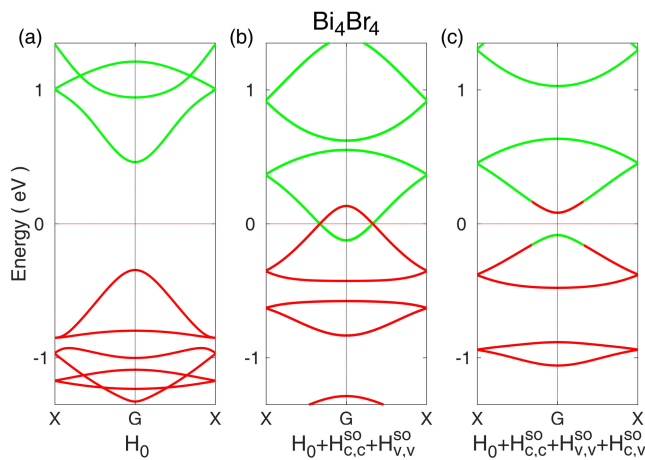
FIG. 2. **Type-I and type-II SOC effects in an HSE+SOC DFT calculation.** Here Bi_4Br_4 is taken as example. (a)-(c) are the band structures of different Hamiltonians. (a) Bands of the Hamiltonian without SOC (H_0), where the red (green) lines represent the valence (conduction) band composition of H_0. (b) Bands perturbed by the strong type-I SOC term, which results in band splittings that make valence (conduction) bands cross Fermi energy. (c) Bands in (b) perturbed further by the type-II SOC term, in which case the gap opens again. Here it is obvious that charge density is changed from (a) to (c), because the valence bands in (c) mix some parts of the previous conduction (green) bands in (a).

TABLE II. Major orbital compositions of the highest valence band and the lowest conduction band for each example material. The orbital compositions listed for WSe_2 are only for band edges at the $K(K')$ point. The p orbital means the collective of p_x, p_y, and p_z orbitals. Bi_{in} and Bi_{ex} mean different Bi atoms located at interior and exterior positions respectively.

	valence band	conduction band
PbI_2	I-p	Pb-p
WSe_2 [33]	$W-d_{xy} \& d_{x^2-y^2}$	$W-d_{z^2}$
$BiOCl$	O-p&Cl-p	Bi-p
$GaSb$	Sb-p	Ga-p
$InSb$	Sb-p	In-p
BiH [17]	$Bi-p_{x,y}$	$Bi-p_{x,y}$
Bi_4I_4 [19]	$Bi_{in}-p_x \& Bi_{ex}-p_x$	$Bi_{in}-p_x \& Bi_{ex}-p_x$
Bi_4Br_4 [19]	$Bi_{in}-p_x \& Bi_{ex}-p_x$	$Bi_{in}-p_x \& Bi_{ex}-p_x$

agrees with the benchmark $H^{\text{HSE+SOC}}$ very well. For these compounds, the properties of their lowest conduction band differ significantly from those of highest valence band, especially in orbital compositions and positions (cf. Table.II). This makes the type-II SOC hopping $\xi_{c,v}^{\text{SO}}$ composed mostly of the SOC interactions between different atoms, and hence $\xi_{c,v}^{\text{SO}}$ are very small. WSe_2 is an exception because its band-edge orbitals locate at the same atom W. However the $W-d_{xy} \& d_{x^2-y^2}$ orbitals have opposite mirror symmetry compared to $W-d_{z^2}$ orbital, which still makes $\xi_{c,v}^{\text{SO}}$ small. Furthermore, the gaps of the normal band insulators are large compared to $\xi_{c,v}^{\text{SO}}$,

TABLE III. **Gap comparison of two Hamiltonians differing by $H_{c,v}^{\text{SO}}$ (in unit of eV).** $H - H_{c,v}^{\text{SO}}$ means the total Hamiltonian with full SOC H excluding $H_{c,v}^{\text{SO}}$, which equals $H_0 + H_{c,c}^{\text{SO}} + H_{v,v}^{\text{SO}}$. $\Delta_{cv} = g(H) - g(H - H_{c,v}^{\text{SO}})$. Gaps listed here are calculated in HSE+SOC case to exemplify the slight effects of the type-II SOC $H_{c,v}^{\text{SO}}$ in the normal band insulators.

	$g(H - H_{c,v}^{\text{SO}})$	$g(H)$	Δ_{cv}	$|\Delta_{cv}|/g(H)$
PbI_2	2.554	2.569	0.015	0.58%
WSe_2	1.604	1.619	0.015	0.93%
$BiOCl$	3.442	3.496	0.054	1.54%
$GaSb$	0.521	0.526	0.005	0.95%
$InSb$	0.171	0.175	0.004	2.29%

i.e. $|\varepsilon_{0v} - \varepsilon_{0c}| \gg |\xi_{c,v}^{\text{SO}}|$. Consequently the perturbed valence band eigenfunction ψ_v can at most slightly mix with the conduction band ψ_{0c} since $\alpha_c \ll 1$ (see Eq. 12), which means type-II SOC has almost no effect. This is shown in table III which illustrates band gaps of $H - H_{c,v}^{\text{SO}}$ and H differ by less than 2.3%. In addition, their band gaps are also large enough compared to the type-I SOC hopping $\xi_{v,v'}^{\text{SO}}$ and $\xi_{c,c'}^{\text{SO}}$, hence this is the weak type-I SOC case which makes no change of charge density if type-II SOC is not considered. We conclude that for normal band insulators, both type-I and type-II SOC effects contribute very little change to the charge density from $\rho_0 = \sum_v \psi_{v0}^* \psi_{v0}$ to $\rho = \sum_v \psi_v^* \psi_v$. This is why that in DFT calculations of these compounds, H_0 of HSE without SOC (H_0^{HSE}) and HSE+SOC ($\tilde{H}_0^{\text{HSE}}$) are very close to each other since charge densities are very close.

Next, we analyze the three compounds where H^{MIX} has significant discrepancy to the benchmark $H^{\text{HSE+SOC}}$. As discussed above, these compounds have inverted bands (BiH, Bi_4Br_4) or near-inverted bands (Bi_4I_4), the orbital compositions of their conduction bands are similar to those of valence bands around the Fermi energy (cf. Table.II). Hence $|\xi_{c,v}^{\text{SO}}|$ is not small in general and can be close to or even larger than $|\varepsilon_{0v} - \varepsilon_{0c}|$. According to Eq.12, this makes α_c not small and the type-II SOC significantly perturb ψ_v. In addition, the large SOC strength of Bi can lead to a strong type-I SOC that make conduction and valence bands cross the Fermi energy [see Fig. 2(b)]. Due to the strong type-I and type-II SOC effects, the charge density changes significantly from ρ_0 to ρ, which makes H_0^{HSE} and $\tilde{H}_0^{\text{HSE}}$ differ from each other.

Quantitatively, we compare the band gaps of H_0^{HSE} and $\tilde{H}_0^{\text{HSE}}$ in Table IV, from which we observe that the gaps of H_0^{HSE} are very close to those of $\tilde{H}_0^{\text{HSE}}$ for PbI_2, $BiOCl$, WSe_2, $GaSb$ and $InSb$, but not so close for Bi_4I_4 and Bi_4Br_4. As a comparison, we also show the gaps of H_0^{PBE} and $\tilde{H}_0^{\text{PBE}} = H_0^{\text{PBE+SOC}} - H_{\text{so}}^{\text{PBE}}$ in Table IV. It should be pointed out that because the PBE gaps without SOC are smaller than HSE gaps, i.e. $|\varepsilon_{v0} - \varepsilon_{c0}|$ are smaller in PBE, ψ_v will mix more ψ_{0c} if $\xi_{c,v}^{\text{SO}}$ and ρ_0 are assumed to be the same in HSE and PBE. Hence the gap differences of PBE are worse than those of HSE for $GaSb$, Bi_4I_4 and

TABLE IV. **Gap comparison of Hamiltonians without SOC (in unit of eV):** H_0^{HSE} **vs** $\tilde{H}_0^{\mathrm{HSE}}$ **as well as** H_0^{PBE} **vs** $\tilde{H}_0^{\mathrm{PBE}}$. Similar to $\tilde{H}_0^{\mathrm{HSE}}$, we define $\tilde{H}_0^{\mathrm{PBE}} = H^{\mathrm{PBE+SOC}} - H_{\mathrm{so}}^{\mathrm{PBE}}$ which means the non-SOC part separated out from the PBE+SOC Hamiltonian. $\Delta_0^{\mathrm{HSE}} = g(H_0^{\mathrm{HSE}}) - g(\tilde{H}_0^{\mathrm{HSE}})$ and $\Delta_0^{\mathrm{PBE}} = g(H_0^{\mathrm{PBE}}) - g(\tilde{H}_0^{\mathrm{PBE}})$. Note that BiH without SOC shows Dirac-cone type of bands with no gaps for comparison, and InSb is calculated to be metallic in PBE without SOC and does not have gaps either.

	$g(\tilde{H}_0^{\mathrm{HSE}})$	$g(H_0^{\mathrm{HSE}})$	Δ_0^{HSE}	$\lvert\Delta_0^{\mathrm{HSE}}\rvert/g(\tilde{H}_0^{\mathrm{HSE}})$	$g(\tilde{H}_0^{\mathrm{PBE}})$	$g(H_0^{\mathrm{PBE}})$	Δ_0^{PBE}	$\lvert\Delta_0^{\mathrm{PBE}}\rvert/g(\tilde{H}_0^{\mathrm{PBE}})$
PbI_2	3.279	3.286	0.007	0.21%	2.529	2.517	−0.012	0.47%
WSe_2	1.996	1.995	−0.001	0.05%	1.554	1.547	−0.007	0.45%
BiOCl	3.722	3.773	0.051	1.37%	2.753	2.782	0.029	1.05%
GaSb	0.773	0.769	−0.004	0.52%	0.123	0.114	−0.009	7.32%
InSb	0.429	0.421	−0.008	1.86%	Metal	Metal	-	-
BiH	Dirac	Dirac	-	-	Dirac	Dirac	-	-
Bi_4I_4	1.050	1.085	0.035	3.33%	0.657	0.610	−0.047	7.15%
Bi_4Br_4	0.806	0.771	−0.035	4.34%	0.408	0.283	−0.125	30.64%

Bi_4Br_4, especially for Bi_4Br_4, as shown in table IV.

B. PBE with SOC

Having understood the discrepancy in the non-SOC part H_0^{HSE} (obtained from HSE without SOC) and $\tilde{H}_0^{\mathrm{HSE}}$, in this subsection we analyze the discrepancy between the SOC part $H_{\mathrm{so}}^{\mathrm{PBE}}$ and $H_{\mathrm{so}}^{\mathrm{HSE}}$. For different XC functionals such as PBE and HSE, there are two major reasons that make H_{so} different in PBE and HSE.

First, according to Eq. 4, different potential energy V makes different SOC parameters. For HSE, its exchange potential $V_{\mathrm{x}}^{\mathrm{HSE}}$ is composed of a short-ranged part $V_{\mathrm{x}}^{\mathrm{SR}}$ and a long-ranged part $V_{\mathrm{x}}^{\mathrm{LR}}$, where $V_{\mathrm{x}}^{\mathrm{SR}}$ is produced by mixing the non-local Fock potential $V_{\mathrm{x}}^{\mathrm{F}}$ (i.e. the exact exchange potential) and the PBE exchange potential $V_{\mathrm{x}}^{\mathrm{PBE}}$ in short range, while $V_{\mathrm{x}}^{\mathrm{LR}}$ is solely the PBE exchange potential $V_{\mathrm{x}}^{\mathrm{PBE}}$ in long range. Since the unscreened Fock potential $V_{\mathrm{x}}^{\mathrm{F}}$ is generally larger than the PBE exchange potential, the resulting $V_{\mathrm{x}}^{\mathrm{HSE}}$ with $V_{\mathrm{x}}^{\mathrm{PBE}}$ replaced partially by the unscreened $V_{\mathrm{x}}^{\mathrm{F}}$, should also be larger than $V_{\mathrm{x}}^{\mathrm{PBE}}$ in general. This is demonstrated by the SOC hopping parameters of HSE and PBE in Fig. 3, in which the HSE ones are consistently larger than the PBE ones. Taking BiH as an example: it has a hexagonal structure like graphane and has Dirac cones at K and K' points in the Brillouin zone without SOC. With SOC, a topological band gap opens at K (K') point and this gap depends only on the strength of SOC. Hence, the larger gap of HSE+SOC than that of our method shown in Fig1(f) means that the SOC strength of HSE+SOC is larger than that of our method, i.e. $H_{\mathrm{so}}^{\mathrm{HSE}}$ is larger than $H_{\mathrm{so}}^{\mathrm{PBE}}$. For other topological insulators similar to BiH, i.e. the ones which have Dirac points or node lines before including SOC, such as $ZrTe_5$[18] and ZrSiO families[20] which have band inversion before considering SOC just as BiH does, they share similar source of discrepancy to BiH in our method[34]. Second, if $\xi_{c,v}^{\mathrm{SO}}$ and ρ_0 of PBE and HSE are assumed to be the same, using the per-

turbation theory, for near-inverse band insulator (Bi_4I_4) or inverse band topological insulator (Bi_4Br_4), different gaps between PBE and HSE make ψ_v mix at different ratios with ψ_{0c}, resulting in different charge densities which gives further differences of V and H_{so} between PBE and HSE.

To quantitatively understand the difference between $H_{\mathrm{so}}^{\mathrm{HSE}}$ and $H_{\mathrm{so}}^{\mathrm{PBE}}$, we compare the gaps of two Hamiltonians: one is $H^{\mathrm{HSE+SOC}}$, and the other is $H^{\mathrm{HSE+SOC}}$ with its SOC part $H_{\mathrm{so}}^{\mathrm{HSE}}$ replaced by $H_{\mathrm{so}}^{\mathrm{PBE}}$, i.e. $\tilde{H}^{\mathrm{MIX}}$ in Table I. We can see from Table I (especially the last column) that the gap differences induced by the difference between $H_{\mathrm{so}}^{\mathrm{HSE}}$ and $H_{\mathrm{so}}^{\mathrm{PBE}}$ are relatively small for band insulators PbI_2, BiOCl, WSe_2, GaSb and InSb, but large for BiH, Bi_4I_4 and Bi_4Br_4.

According to these analyses, for normal band insulators, the differences between H_0^{HSE} and $\tilde{H}_0^{\mathrm{HSE}}$ are as small as the differences between $H_{\mathrm{so}}^{\mathrm{HSE}}$ and $H_{\mathrm{so}}^{\mathrm{PBE}}$. This is why our method works so wy our method works so well for the five compounds PbI_2, WSe_2, BiOCl, GaSb and InSb (see Table I). But for the three near-inverse and inverse band insulators BiH, Bi_4I_4 and Bi_4Br_4, the differences between $H_{\mathrm{so}}^{\mathrm{HSE}}$ and $H_{\mathrm{so}}^{\mathrm{PBE}}$ are much larger [cf. the $\lvert\Delta_0^{\mathrm{HSE}}\rvert/g(\tilde{H}_0^{\mathrm{HSE}})$ column in table IV and the $\lvert\Delta_2\rvert/g(H_{\mathrm{+SOC}}^{\mathrm{HSE}})$ column in table I]. Furthermore, by comparing Δ_1 and Δ_2 in Table I, we conclude that the error of our method is dominated by the difference between $H_{\mathrm{so}}^{\mathrm{HSE}}$ and $H_{\mathrm{so}}^{\mathrm{PBE}}$, and this error are large for the near-inverse and inverse band insulators. Note, however, although the *relative* deviation of our H^{MIX} with respect to $H^{\mathrm{HSE+SOC}}$ is large for Bi_4I_4 and Bi_4Br_4, their *absolute* deviations are actually not large, as illustrated by the not-so-large differences of the SOC hopping parameters between PBE and HSE shown in Fig.3.

We therefore conclude that our method is a very good approximation for normal band insulators and, for near-inverse or inverse band insulators which have very small band gaps, our method is still reasonable in that it can provide qualitatively correct results.
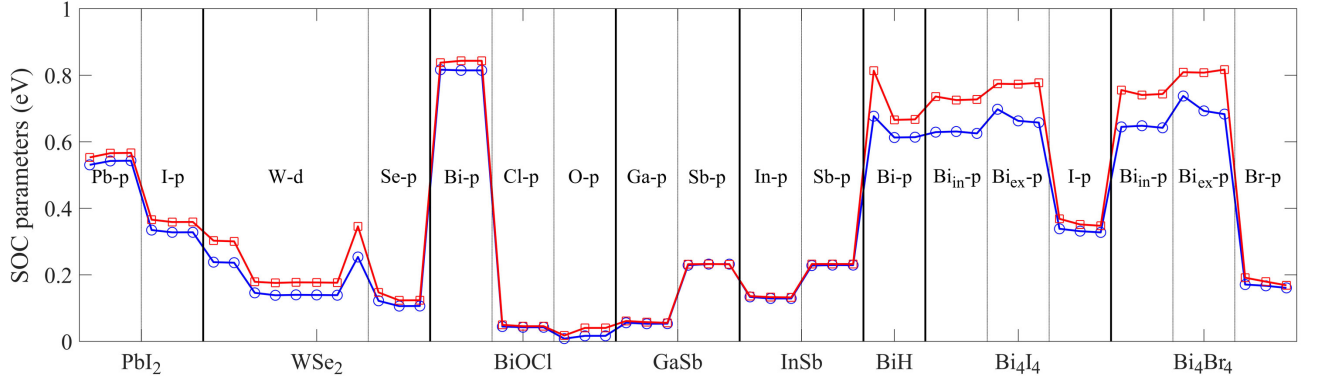
FIG. 3. **On site SOC parameters in Hamiltonian.** The blue circles (red squares) are from PBE+SOC (HSE+SOC), and lines are provided to guide the eye. For p-orbitals, three circles (squares) mean $\left|\left\langle p_x^\uparrow \left|\widehat{H}_{\mathrm{so}}\right| p_y^\uparrow \right\rangle\right|$, $\left|\left\langle p_y^\uparrow \left|\widehat{H}_{\mathrm{so}}\right| p_z^\downarrow \right\rangle\right|$ and $\left|\left\langle p_z^\uparrow \left|\widehat{H}_{\mathrm{so}}\right| p_x^\downarrow \right\rangle\right|$ respectively. For d-orbitals of W in the figure, eight circles (squares) mean $\left|\left\langle d_{z^2}^\uparrow \left|\widehat{H}_{\mathrm{so}}\right| d_{xz}^\downarrow \right\rangle\right|$, $\left|\left\langle d_{z^2}^\uparrow \left|\widehat{H}_{\mathrm{so}}\right| d_{yz}^\downarrow \right\rangle\right|$, $\left|\left\langle d_{xz}^\uparrow \left|\widehat{H}_{\mathrm{so}}\right| d_{yz}^\uparrow \right\rangle\right|$, $\left|\left\langle d_{xz}^\uparrow \left|\widehat{H}_{\mathrm{so}}\right| d_{x^2-y^2}^\downarrow \right\rangle\right|$, $\left|\left\langle d_{xz}^\uparrow \left|\widehat{H}_{\mathrm{so}}\right| d_{xy}^\downarrow \right\rangle\right|$, $\left|\left\langle d_{yz}^\uparrow \left|\widehat{H}_{\mathrm{so}}\right| d_{x^2-y^2}^\downarrow \right\rangle\right|$, $\left|\left\langle d_{yz}^\uparrow \left|\widehat{H}_{\mathrm{so}}\right| d_{xy}^\downarrow \right\rangle\right|$, and $\left|\left\langle d_{x^2-y^2}^\uparrow \left|\widehat{H}_{\mathrm{so}}\right| d_{xy}^\uparrow \right\rangle\right|$ respectively. $\mathrm{Bi_{in}}$ and $\mathrm{Bi_{ex}}$ mean Bi atoms in different positions [19]. It should be pointed out that the orbitals here are the orthonormalized orbitals (see eq. A13 in Appendix A).

C. Discussions

The purpose of this work is to develop a reasonably accurate, qualitatively correct and computationally efficient method to perform HSE+SOC calculations within DFT. We have so far demonstrated the accuracy of our method and understood the source of discrepancy when dealing with near-inverse and inverse band insulators.

Concerning computational efficiency: our method for HSE+SOC calculation takes essentially the same time as an HSE calculation without SOC. Taking WSe$_2$ for example, in our calculations, one PBE+SOC electronic step takes 1.3 minute using 32 CPU cores, one HSE (without SOC) electronic step takes 5.6 minute using 128 CPU cores, and one full HSE+SOC electronic step takes 50.5 minute using 128 CPU cores. Therefore our technique is nearly an order of magnitude faster than the full HSE+SOC calculation. We checked that for all the cases we investigated, our method is faster by several times to more than an order of magnitude that the full direct HSE+SOC approach.

So far we analyzed non-magnetic compounds, but the method can be easily extended to magnetic materials for which $H_0^\uparrow$ and $H_0^\downarrow$ are not equal anymore but can be obtained in an additional spin-colinear DFT calculation. Namely, our method can be extended to magnetic materials by performing a spin-colinear PBE calculation and a PBE+SOC calculation to extract $H_{\mathrm{so}}^{\mathrm{PBE}}$; then performing a spin-colinear HSE calculation to obtain H_0^{HSE}. The results are added together to obtain H^{MIX} for the magnetic material.

The method developed in this work is not only suitable for LCAO, but also useful for accelerating HSE+SOC DFT calculations. Usually, two initializations are used

to save computing time during HSE+SOC calculations: (a) using charge density and wave function from a PBE+SOC calculation as initialization, (b) using charge density and wave function from a HSE calculation without SOC as initialization. However, both will actually not accelerate calculation significantly. This is because for (a), H_0 of PBE+SOC differ quite a lot from that of HSE+SOC; and for (b), it lacks H_{so}. Then, naturally, our method provides a better starting charge density and wave functions for full HSE+SOC DFT calculation because H^{MIX} is closer to $H^{\mathrm{HSE+SOC}}$ than $H^{\mathrm{PBE+SOC}}$ or H_0^{HSE}.

IV. SUMMARY

In summary, we have developed an efficient mixed LCAO technique to perform HSE+SOC DFT calculations. The LCAO Hamiltonian is obtained by mixing a non-SOC part and an SOC part. The non-SOC part is constructed by SOC-free HSE, and the SOC part by PBE+SOC. As a result, the mixed LCAO technique requires a computing time comparable to that of a non-SOC HSE calculation, thus saving about one order magnitude in computing time compared to a full direct HSE+SOC calculation.

Applying the method to eight non-magnetic compounds demonstrates that the mixed LCAO Hamiltonian can well approximate that of the full HSE+SOC. In particular, the method works very well for normal band insulators, and it is also reasonable to give qualitatively correct results for near-inverse and inverse band insulators having very small band gaps. We find that the errors in our method came from the difference between $H_{\mathrm{so}}^{\mathrm{HSE}}$

and $H_{\text{so}}^{\text{PBE}}$ more than the difference between $\tilde{H}_0^{\text{HSE}}$ and H_0^{HSE} in most cases. Our method can be easily extended to other hybrid functionals and magnetic materials, and it can also be used to provide good initial conditions for full direct HSE+SOC calculation.

V. ACKNOWLEDGMENTS

Appendix A: LCAO representation and interpolation

Using VASP2WANNIER90 [28–30], we can project the local orbitals $g_n(\boldsymbol{r})$ onto the Bloch manifold $\psi_{m\boldsymbol{k}}$ determined by VASP at wave vector $\boldsymbol{k}$ to obtain

$$|\varphi_{n\boldsymbol{k}}\rangle \equiv \sum_{m=1}^{N_b} |\psi_{m\boldsymbol{k}}\rangle \langle \psi_{m\boldsymbol{k}}| g_n\rangle, \qquad (A1)$$

$$A_{mn}^{\boldsymbol{k}} \equiv \langle \psi_{m\boldsymbol{k}}| g_n\rangle, \qquad (A2)$$

where g_n is localized trial orbitals serving as the initial guess of the Wannier functions, and N_b is the number of bands considered or the dimension of the Bloch manifold at $\boldsymbol{k}$. Thus obtained $|\varphi_{n\boldsymbol{k}}\rangle$ are only determined by the local orbitals g_n, for $|\varphi_{n\boldsymbol{k}}\rangle$ can be Fourier transformed to $g_n^{\boldsymbol{R}}(\boldsymbol{r}) \equiv g_n(\boldsymbol{r}-\boldsymbol{R})$ in which $\boldsymbol{R}$ is lattice vector. To show this, first apply the Bloch theorem $\varphi_{n\boldsymbol{k}}(\boldsymbol{r}-\boldsymbol{R}) = e^{-i\boldsymbol{k}\cdot\boldsymbol{R}}\varphi_{n\boldsymbol{k}}(\boldsymbol{r})$ to eq. A1 to get

$$|\varphi_{n\boldsymbol{k}}\rangle = e^{i\boldsymbol{k}\cdot\boldsymbol{R}} \sum_{m=1}^{N_b} |\psi_{m\boldsymbol{k}}\rangle \langle \psi_{m\boldsymbol{k}}| g_n^{\boldsymbol{R}}\rangle, \qquad (A3)$$

and then do Fourier transformation to get

$$\frac{1}{N} \sum_{\boldsymbol{k}} e^{-i\boldsymbol{k}\cdot\boldsymbol{R}} |\varphi_{n\boldsymbol{k}}\rangle$$
$$= \frac{1}{N} \sum_{m\boldsymbol{k}} |\psi_{m\boldsymbol{k}}\rangle \langle \psi_{m\boldsymbol{k}}| g_n^{\boldsymbol{R}}\rangle = |g_n^{\boldsymbol{R}}\rangle \qquad (A4)$$

where N is the number of unit cells (also the number of $\boldsymbol{k}$ points). In the above equation, we have used the completeness relation

$$\frac{1}{N} \sum_{m\boldsymbol{k}} |\psi_{m\boldsymbol{k}}\rangle \langle \psi_{m\boldsymbol{k}}| = 1 \qquad (A5)$$

due to the normalization convention $\langle \psi_{m\boldsymbol{k}}| \psi_{n\boldsymbol{k'}}\rangle = N\delta_{mn}\delta_{\boldsymbol{k}\boldsymbol{k'}}$ [29]. The inverse transformation of eq. A4 shows that $|\varphi_{n\boldsymbol{k}}\rangle$ is just the Bloch sum of g_n:

$$|\varphi_{n\boldsymbol{k}}\rangle = \sum_{\boldsymbol{R}} e^{i\boldsymbol{k}\cdot\boldsymbol{R}} g_n^{\boldsymbol{R}}. \qquad (A6)$$

Under the bases of $|\varphi_{n\boldsymbol{k}}\rangle$, the Hamiltonian matrix is $\mathcal{H}^{\boldsymbol{k}} = A^{\boldsymbol{k}\dagger}\mathcal{E}^{\boldsymbol{k}}A^{\boldsymbol{k}}$ with matrix elements

$$\begin{aligned}\mathcal{H}_{ij}^{\boldsymbol{k}} &= \langle \varphi_{i\boldsymbol{k}}| \hat{H} |\varphi_{j\boldsymbol{k}}\rangle \\ &= \frac{1}{N^2} \sum_{m,n} \langle \varphi_{i\boldsymbol{k}}| \psi_{m\boldsymbol{k}}\rangle \langle \psi_{m\boldsymbol{k}}| \hat{H} |\psi_{n\boldsymbol{k}}\rangle \langle \psi_{n\boldsymbol{k}}| \varphi_{j\boldsymbol{k}}\rangle \\ &= \sum_{m,n} A_{im}^{\boldsymbol{k}\dagger} \mathcal{E}_{mn}^{\boldsymbol{k}} A_{nj}^{\boldsymbol{k}} \end{aligned} \qquad (A7)$$

in which $\mathcal{E}_{mn}^{\boldsymbol{k}} = \delta_{mn}\varepsilon_{n\boldsymbol{k}}$ and $\varepsilon_{n\boldsymbol{k}}$ is the eigenenergy of the Bloch state $|\psi_{n\boldsymbol{k}}\rangle$. In the above equation, eq. A5 and the relation $\langle \psi_{n\boldsymbol{k}}| \varphi_{j\boldsymbol{k}}\rangle = NA_{nj}^{\boldsymbol{k}}$ (see eq. A1 and A2) are used. Because $g_n^{\boldsymbol{R}}$ and hence $|\varphi_{n\boldsymbol{k}}\rangle$ are not orthonormalized, the eigen equation of $\mathcal{H}^{\boldsymbol{k}}$ is

$$\mathcal{H}^{\boldsymbol{k}}\phi = \varepsilon S^{\boldsymbol{k}}\phi \qquad (A8)$$

where the overlap matrix $S^{\boldsymbol{k}}$ is defined by

$$S_{ij}^{\boldsymbol{k}} = \frac{1}{N} \langle \varphi_{i\boldsymbol{k}}| \varphi_{j\boldsymbol{k}}\rangle = \left(A^{\boldsymbol{k}\dagger}A^{\boldsymbol{k}}\right)_{ij}. \qquad (A9)$$

To orthonormalize the bases, we construct $\tilde{\varphi}_{n\boldsymbol{k}}$ with properties $\langle \tilde{\varphi}_{m\boldsymbol{k}}| \tilde{\varphi}_{n\boldsymbol{k}}\rangle = N\delta_{mn}$ as follows

$$|\tilde{\varphi}_{n\boldsymbol{k}}\rangle = \sum_{m=1}^{N_b} |\varphi_{m\boldsymbol{k}}\rangle T_{mn}^{\boldsymbol{k}} \qquad (A10)$$

in which $T^{\boldsymbol{k}}$ is a Hermitian matrix with the property $(T^{\boldsymbol{k}})^2 = (S^{\boldsymbol{k}})^{-1}$ and hence can be denoted as $T^{\boldsymbol{k}} = (S^{\boldsymbol{k}})^{-\frac{1}{2}}$ in form. The existence of $T^{\boldsymbol{k}}$ is guaranteed by the Hermiticity of $S^{\boldsymbol{k}}$. As a result, the Hamiltonian matrix under the orthonormalized bases $|\tilde{\varphi}_{m\boldsymbol{k}}\rangle$ is

$$H(\boldsymbol{k}) = T^{\boldsymbol{k}\dagger}\mathcal{H}^{\boldsymbol{k}}T^{\boldsymbol{k}} = (A^{\boldsymbol{k}}T^{\boldsymbol{k}})^{\dagger}\mathcal{E}^{\boldsymbol{k}}A^{\boldsymbol{k}}T^{\boldsymbol{k}}, \qquad (A11)$$

which can be constructed from the data $\varepsilon_{m\boldsymbol{k}}$ and $A_{mn}^{\boldsymbol{k}}$ generated by VASP and VASP2WANNIER90 respectively.

Because $\varphi_{m\boldsymbol{k}}$ are determined only by g_n (eq. A6), $S^{\boldsymbol{k}}$ is determined only by $\varphi_{m\boldsymbol{k}}$ (eq. A9), $T^{\boldsymbol{k}}$ is determined only by $S^{\boldsymbol{k}}$, and $\tilde{\varphi}_{m\boldsymbol{k}}$ are determined only by $\varphi_{m\boldsymbol{k}}$ and $T^{\boldsymbol{k}}$ (eq. A10), it can be concluded that the final bases $\tilde{\varphi}_{m\boldsymbol{k}}$ are only determined by the initial local orbitals g_n

and irrelevant to the Bloch states $\psi_{m\boldsymbol{k}}$. This is crucial for us to add directly H_0^{HSE} and $H_{\mathrm{so}}^{\mathrm{PBE}}$ constructed from independent DFT calculations, because H_0^{HSE} and $H_{\mathrm{so}}^{\mathrm{PBE}}$ have the same bases $\tilde{\varphi}_{m\boldsymbol{k}}$ as long as the same initial local orbitals g_n are used.

The obtained $H(\boldsymbol{k})$ from eq. A11 is defined at only a finite number (N) of $\boldsymbol{k}$ points. If the Hamiltonian at an arbitrary wave vector $\boldsymbol{q}$ different from the N $\boldsymbol{k}$ points is required, interpolation has to be done. The interpolation can be achieved through two steps. First, do a Fourier transformation for $H(\boldsymbol{k})$ to get the Hamiltonian element in real space

$$H_{nm}^{\boldsymbol{R}} = \langle \boldsymbol{0}n| \widehat{H} |\boldsymbol{R}m\rangle = \frac{1}{N} \sum_{\boldsymbol{k}} e^{-i\boldsymbol{k}\cdot\boldsymbol{R}} H_{nm}(\boldsymbol{k}). \quad \text{(A12)}$$

in which $|\boldsymbol{R}m\rangle$ is the Fourier transformation of $|\tilde{\varphi}_{m\boldsymbol{k}}\rangle$

$$|\boldsymbol{R}m\rangle = \frac{1}{N} \sum_{\boldsymbol{k}} e^{-i\boldsymbol{k}\cdot\boldsymbol{R}} |\tilde{\varphi}_{m\boldsymbol{k}}\rangle \quad \text{(A13)}$$

and is an orthonormalized local orbital with property $\langle \boldsymbol{R}n| \boldsymbol{R}'m\rangle = \delta_{\boldsymbol{R}\boldsymbol{R}'}\delta nm$. Then, construct the Hamiltonian at arbitrary wave vector $\boldsymbol{q}$ using the $\boldsymbol{k}$-indepnedent quantities $H_{nm}^{\boldsymbol{R}}$ as follows :

$$H_{nm}(\boldsymbol{q}) = \sum_{\boldsymbol{R}} e^{i\boldsymbol{q}\cdot\boldsymbol{R}} H_{nm}^{\boldsymbol{R}}. \quad \text{(A14)}$$

We call this procedure LCAO interpolation.

Appendix B: The weak type-I SOC effect

To interpret the effect of the type-I SOC, we consider the Hamiltonian eq. 11 in the absence of type-II SOC hoppings $\xi_{c,v}^{\mathrm{SO}}$

$$\begin{aligned} H = &\sum_c \varepsilon_{0c} a_c^\dagger a_c + \sum_v \varepsilon_{0v} a_v^\dagger a_v \\ &+ \sum_{c,c'} \xi_{c,c'}^{\mathrm{SO}} a_c^\dagger a_{c'} + \sum_{v,v'} \xi_{v,v'}^{\mathrm{SO}} a_v^\dagger a_{v'}, \quad \text{(B1)} \end{aligned}$$

in which $v, v' = 1, \cdots, N_{\mathrm{v}}$ represent valence bands, $c, c' = N_{\mathrm{v}}+1, \cdots, N_{\mathrm{b}}$ represent conduction bands, N_{v} and N_{c} are the number of valence and conduction bands respectively, and $N_{\mathrm{b}} = N_{\mathrm{v}} + N_{\mathrm{c}}$ is the total number of bands considered. Note that the spin index is incorporated into the band index v and c here for simplicity. Choosing the eigen states $\psi_{0c/v}$ of H_0 as bases, H_0 is a diagonal matrix $H_0 = \mathrm{diag}\{H_0^{\mathrm{v}}, H_0^{\mathrm{c}}\}$ with

$$H_0^{\mathrm{v}} = \mathrm{diag}\{\varepsilon_{01}, \cdots, \varepsilon_{0N_{\mathrm{v}}}\}, \quad \text{(B2)}$$

$$H_0^{\mathrm{c}} = \mathrm{diag}\{\varepsilon_{0,N_{\mathrm{v}}+1}, \cdots, \varepsilon_{0N_{\mathrm{b}}}\}, \quad \text{(B3)}$$

and H_{so} is a block-diagonal matrix $H_{\mathrm{so}} = \mathrm{diag}\{H_{\mathrm{so}}^{\mathrm{v}}, H_{\mathrm{so}}^{\mathrm{c}}\}$ with $H_{\mathrm{so}}^{\mathrm{v}}$ and $H_{\mathrm{so}}^{\mathrm{c}}$ being $N_{\mathrm{v}} \times N_{\mathrm{v}}$ and $N_{\mathrm{c}} \times N_{\mathrm{c}}$ matrices respectively. Hence, the charge density of H_0 is

$$\rho_0 = \sum_{v=1}^{N_{\mathrm{v}}} |\psi_{0v}|^2 = \sum_{v=1}^{N_{\mathrm{v}}} |\psi_v|^2, \quad \text{(B4)}$$

where ψ_v is the eigen state of $H_{\mathrm{v}} = H_0^{\mathrm{v}} + H_{\mathrm{so}}^{\mathrm{v}}$ and the second equality is due to the fact that ψ_v is related to ψ_{0v} by a unitary transformation U with $\psi_v = \sum_{v'} \psi_{0v'} U_{v'v}$ and $U_{v'v} = \langle \psi_{0v'}| \psi_v\rangle$ (For simplicity we use the usual normalization convention $\langle \psi_{0v}| \psi_{0v'}\rangle = \langle \psi_v| \psi_{v'}\rangle = \delta_{vv'}$ here). This is guaranteed by the absence of type-II SOC hoppings $\xi_{c,v}^{\mathrm{SO}}$.

If the type-I SOC effect is weak, H_{so} will not make conduction or valence bands cross the Fermi energy like Fig. 2(b). This makes the charge density of $H = H_0 + H_{\mathrm{so}}$ is just determined by the valence bands ψ_v

$$\rho = \sum_{v=1}^{N_{\mathrm{v}}} |\psi_v|^2. \quad \text{(B5)}$$

Considering eq. B4 we have

$$\rho = \rho_0. \quad \text{(B6)}$$

Therefore, the weak type-I SOC effect cannot make difference between the charge densities ρ and ρ_0.

---

[*] gbliu@bit.edu.cn
[†] ygyao@bit.edu.cn

[1] W. Kohn, Int. J. Quantum Chem. **56**, 229 (1995).
[2] J. P. Perdew, M. Ernzerhof, and K. Burke, J. Chem. Phys. **105**(22), 9982 (1996) .
[3] M. Ernzerhof, J. P. Perdew, and K. Burke, Int. J. Quantum Chem. **64**, 285 (1997).
[4] M. Ernzerhof and G. E. Scuseria, J. Chem. Phys. **110**, 5029 (1999).
[5] C. Adamo and V. Barone, J. Chem. Phys. **110**(13), 6158 (1999).
[6] J. Heyd, G. E. Scuseria and M. J. Ernzerhof, Chem. Phys. **118**, 8207 (2003).
[7] J. Heyd and G. E. Scuseria, J. Chem. Phys. **121**, 1187 (2004).
[8] J. Heyd, G. E. Scuseria, and M. Ernzerhof,, J. Chem. Phys. **124**, 219906 (2006).
[9] A. V. Krukau, O. A. Vydrov, A. F. Izmaylov, and G. E. Scuseria, J. Chem. Phys. **125**, 224106 (2006).
[10] M. Z. Hasan and C. L. Kane, Rev. Mod. Phys. **82**, 3045 (2010).
[11] X.-L. Qi and S.-C. Zhang, Rev. Mod. Phys. **83**, 1057 (2011).
[12] H. Zhang, C.-X. Liu, X.-L. Qi, X. Dai, Z. Fang and S.-C. Zhang, Nat. Phys. **5**, 438 (2009).
[13] C.-C. Liu, W. Feng, and Y. Yao, Phys. Rev. Lett. **107**, 076802 (2011).

[14] C. C. Liu, H. Jiang, and Y. G. Yao, Phys. Rev. B **84**, 195430 (2011).

[15] Y. Xu, B. Yan, H.-J. Zhang, J. Wang, G. Xu, P. Tang, W. Duan, and S.-C. Zhang, Phys. Rev. Lett. **111**, 136804 (2013).

[16] Z. Song, C.-C. Liu, J. Yang, J. Han, M. Ye, B. Fu, Y. Yang, Q. Niu, J. Lu, and Y. G. Yao, NPG Asia Materials **6**, e147 (2014).

[17] C.-C. Liu, S. Guan, Z. Song, S. A. Yang, J. Yang, and Y. G. Yao, Phys. Rev. B **90**, 085431 (2014).

[18] H. Weng, X. Dai and Z. Fang, Phys. Rev. X **4**, 011002 (2014).

[19] J.-J. Zhou, W. Feng, C.-C. Liu, S. Guan, and Y. Yao, Nano Lett. **14**, 4767 (2014).

[20] Q. Xu, Z. Song, S. Nie, H. Weng, Z. Fang and X. Dai, Phys. Rev. B **92**, 205310 (2015).

[21] M. Zhou, W. Duan, Y. Chen and A. Du, Nanoscale **7**, 15168 (2015).

[22] K.-L. Zhang, C.-M. Liu, F.-Q. Huang, C. Zheng and W.-D. Wang, Appl. Cata. B: Envi. **68(3)**, 125 (2006).

[23] G.-B. Liu, D. Xiao, Y. Yao, X. Xude and W. Yao, Chem. Soc. Rev. **44**, 2643 (2015).

[24] Y.-S. Kim, M. Marsman, G. Kresse, F. Tran, and Peter Blaha, Phys. Rev. B **82**, 205212 (2010).

[25] G. Kresse, and J. Furthmüller, Phys. Rev. B **54**, 11169 (1996).

[26] J. P. Perdew, K. Burke, and M. Ernzerhof, Phys. Rev. Lett. **77**, 3865 (1996).

[27] G. Kresse, and D. Joubert, Phys. Rev. B **59**, 1758 (1999).

[28] A. A. Mostofi, J. R. Yates, Y.-S. Lee, I. Souza, D. Vanderbilt and N. Marzari, Comput. Phys. Commun. **178**, 685 (2008).

[29] N. Marzari, A. A. Mostofi, J. R. Yates, I. Souza and D. Vanderbilt, Rev. Mod. Phys. **84**, 1419 (2012).

[30] C. Franchini, R. Ková čik, M. Marsman, S. Sathyanarayana Murthy, J. He, C. Ederer, and G. Kresse,J. Phys.: Condens. Matter **24**, 235602 (2012).

[31] Since HSE has non-local Fock potential included, which depends on ground state wave function, the difference between ground state wave functions calculated by the two approaches will also cause the discrepancy. However, ground state wave function plays a similar role of ground state electronic density, so we do not discuss it individually.

[32] Conduction (valence) band here means unoccupied (occupied) band without considering SOC.

[33] G.-B. Liu, W.-Y. Shan, Y. Yao, W. Yao, and D. Xiao, Phys. Rev. B **88**, 085433 (2013).

[34] Calculations show that the band-structure discrepancies introduced in our method for $ZrTe_5$ and ZrSiO are obviously smaller than for BiH due to smaller SOC strength of Zr and Te atoms than Bi atom.